ROME 2008
LEVERAGING TECHNOLOGY

P346

Effective Reflection Coefficients for Curved Interfaces in TI Media

M. Ayzenberg* (Norwegian University of Science and Technology), I. Tsvankin (Colorado School of Mines), A. Aizenberg (Institute of Petroleum Geology and Geophysics) & B. Ursin (Norwegian University of Science and Technology)

SUMMARY

We introduce so-called effective reflection coefficients (ERC) for curved interfaces in transversely isotropic media. If the reflector is plane, ERC describe the exact reflected wavefield for the full range of incidence angles, while plane-wave reflection coefficients become inadequate at near-critical and post-critical angles. For curved reflectors, ERC provide a practical way of computing the wavefield without using such time-consuming methods as finite differences. We analyze parameter dependence of ERC and evaluate the potential of using them in amplitude-versus-offset inversion and Kirchhoff-type modeling.

Introduction. Plane-wave reflection coefficients (PWRC) and their weak-contrast, weak-anisotropy approximations have been extensively used in amplitude-versus-offset (AVO) studies of conventional-spread data (Rüger, 2002; Tsvankin, 2005). These approximations, however, become inadequate at near-critical and post-critical angles, as well as in the presence of reflector curvature (van der Baan and Smit, 2006). Under these circumstances, we propose to use so-called "effective" reflection coefficients (ERC), because they generalize the plane-wave coefficients for wavefields from point sources at curved interfaces (Ayzenberg et al., 2007). We extend ERC, which were previously introduced for acoustic models, to transversely isotropic (TI) layers with curved boundaries. We evaluate the potential of using the ERC in AVO inversion, and show their advantages in Kirchhoff-type modeling.

Generalized plane-wave decomposition of PP and PS reflected wavefields. We consider a 3D model with a curved smooth reflector separating homogeneous isotropic and TI media (see a 2D sketch in Figure 1). The symmetry axis in the TI medium is assumed to be orthogonal to the reflector at each point.

For a plane interface, the reflected PP or PS wavefield $\mathbf{u}_{PQ}(\mathbf{x})$ (index Q denotes the P or S mode) at point $\mathbf{x}$ of the interface $z=0$ can be found as the spectral integral over plane waves (e.g., Tsvankin, 2005):

$$\mathbf{u}_{PQ}(\mathbf{x}) = \frac{1}{2\pi}\int_{-\infty}^{+\infty}\int_{-\infty}^{+\infty} R_{PQ}(\mathbf{p})\,\mathbf{U}_P^{inc}(\mathbf{p})\,e^{i\omega\left(p_x x + p_y y\right)}dp_x\,dp_y\,,$$

where $R_{PQ}(\mathbf{p})$ is the plane-wave reflection or conversion coefficient (Rüger, 2002), $\mathbf{p}=(p_x,p_y)$ is the horizontal projection of the slowness vector, and $\mathbf{U}_P^{inc}(\mathbf{p})$ is the known spatial spectrum of the incident spherical P-wave $\mathbf{u}_P^{inc}(\mathbf{x})$.

In the case of a curved interface, the reflected wavefield $\mathbf{u}_{PQ}(\mathbf{x})$ at the interface can be represented by the spectral integral over generalized plane waves discussed by Klem-Musatov et al. (2004) and Ayzenberg et al. (2007). The generalized plane-wave decomposition of the incident P-wave $\mathbf{u}_P^{inc}(\mathbf{x})$ can be applied only locally using curvilinear surface coordinates, and $\mathbf{p}=(p_x,p_y)$ becomes the projection of the slowness vector on the plane tangential to the interface. Therefore, the spatial spectrum $\mathbf{U}_P^{inc}(\mathbf{p})$ depends on the local reflector geometry, and no longer represents an explicit analytic function. The spectrum $\mathbf{U}_P^{inc}(\mathbf{p})$ naturally incorporates information about the local reflector geometry into the wavefield $\mathbf{u}_{PQ}(\mathbf{x})$.

Effective reflection coefficients. Because of the azimuthal symmetry with respect to the local reflector normal, we need to consider only the normal and tangential components of the PP or PS reflected wavefield. Thus, we define the normal $\chi_{PQ,n}(\mathbf{x})$ and tangential $\chi_{PQ,t}(\mathbf{x})$ ERC as

$$\chi_{PQ,n}(\mathbf{x}) = u_{PQ,n}(\mathbf{x})/u_{P,n}^{inc}(\mathbf{x}),\quad \chi_{PQ,t}(\mathbf{x}) = u_{PQ,t}(\mathbf{x})/u_{P,t}^{inc}(\mathbf{x}).$$

For typical seismic frequencies, the ERC for a curved reflector can be reduced to the ERC for an "equivalent" model with a plane interface tangential to the actual reflector and a new "apparent" source position (Ayzenberg et al., 2007). The distance between the apparent source and the plane interface is

$$R^* = R/\left\{1 - R\,H\,\cos\theta/\left[1-0.5\sin^2\theta\right]\right\},$$

where R is the distance from the actual source to point $\mathbf{x}$, H is the mean interface curvature, and θ is the incidence angle (Figure 2). This formula shows how the local reflector

curvature is included in the ERC. If the reflector is locally plane, we set $H=0$, and R^* reduces to R. For particular parameter combinations, the distance R^* may go to infinity, which means that the incident wave appears to be locally plane; in that case, the ERC reduces to the PWRC. For some values of the product RH, R^* may become negative. Then the apparent source becomes the focus of an apparent converging spherical wave, and the ERC becomes complex conjugate.

In contrast to PWRC, which depend on the model parameters and incidence angle θ, ERC are controlled by one more dimensionless parameter, $L=\omega R^*/V_{P1}$. As an example, the vertical PP and PS ERC for a wide range of L are shown in Figures 3 and 4. Here, the interface is a horizontal plane located 1 km below the source. The P-wave velocity in the upper medium is $V_{P1}=2.0$ km/s, S-wave velocity is $V_{S1}=1.2$ km/s, and density is $\rho_1=2.15$ g/cm^3. The vertical P-wave velocity in the lower medium is $V_{P2}(0)=3.0$ km/s, vertical S-wave velocity is $V_{S2}(0)=1.7$ km/s, density is $\rho_2=2.35$ g/cm^3, and Thomsen parameters are $\varepsilon=\delta=0.1$. The ERC reduces to the corresponding PWRC when $L=\infty$ (see the result for $L=10^4$). The largest differences between the ERC and the PWRC are observed for $L=10$. The ERC oscillates in the post-critical domain due to the interference of the reflected and head waves. One might notice that at zero offset the reflected PS wave does not vanish, which contradicts the geometrical seismics. Due to space limitations, here we do not analyze the dependence of ERC on the interface geometry and anisotropy coefficients.

Because ERC represent the exact solution for plane reflectors, they can improve AVO inversion of long-offset PP data (Skopintseva et al., 2007). For curved reflectors, ERC gives an approximate reflection response, which is difficult to obtain using other methods. In addition to application in AVO studies, ERC may be used for estimation of such geometrical parameters as the depth and local curvature of reflectors.

Effective reflection coefficients in Kirchhoff-type modeling. The reflected wavefield at receiver $\mathbf{x}$ can be represented by a Kirchhoff-type surface integral,

$$\mathbf{u}_{PQ}(\mathbf{x})=\iint_S\left\{\left[\mathbf{N}(\mathbf{x}')\cdot\mathbf{u}_{PQ}(\mathbf{x}')\right]\cdot\mathbf{G}(\mathbf{x}',\mathbf{x})-\mathbf{u}_{PQ}(\mathbf{x}')\cdot\left[\mathbf{n}(\mathbf{x}')\cdot\Sigma(\mathbf{x}',\mathbf{x})\right]\right\}dS(\mathbf{x}'),$$

where $\mathbf{G}(\mathbf{x}',\mathbf{x})$ and $\Sigma(\mathbf{x}',\mathbf{x})$ are the Green's displacement and stress tensors, $\mathbf{N}(\mathbf{x}')$ is the differential traction operator, and $\mathbf{n}(\mathbf{x}')$ is the normal to the interface S. For a homogeneous medium and a smooth interface, the Green's tensors $\mathbf{G}(\mathbf{x}',\mathbf{x})$ and $\Sigma(\mathbf{x}',\mathbf{x})$ are known analytic functions. The boundary values of the reflected wavefield $\mathbf{u}_{PQ}(\mathbf{x}')$ at the interface are calculated as the product of the incident wavefield component ($u^{inc}_{P,n}(\mathbf{x}')$ or $u^{inc}_{P,t}(\mathbf{x}')$) and the corresponding ERC ($\chi_{PQ,n}(\mathbf{x}')$ or $\chi_{PQ,t}(\mathbf{x}')$). For comparison with conventional Kirchhoff modeling, the boundary values of the reflected wavefield $\mathbf{u}_{PQ}(\mathbf{x}')$ are also calculated with the PWRC $R_{PQ}(\mathbf{p})$, in accordance with the geometrical seismics.

Figures 5 and 6 display modeling results for an isotropic medium over a bending TI layer. The model parameters are $V_{P1}=3.0$ km/s, $V_{S1}=1.7$ km/s, $\rho_1=2.15$ g/cm^3, $V_{P2}(0)=4.0$ km/s, $V_{S2}(0)=2.3$ km/s, $\rho_2=2.35$ g/cm^3, $\varepsilon=0.22$ and $\delta=0.1$. The reflector has a flexural shape along the x-direction and is defined as $z=-1.185+0.2\tanh\left[2\pi\left(x-0.75\right)\right]$ km. The

source is at point $x = z = 0$ km, and the receiver array is horizontal at $z = -0.585$ km. The 2D isotropic analog of this model was used by several authors for testing finite-difference modeling and generalized ray tracing (Hanyga and Helle, 1995).

The vertical component of the reflected wavefield in Figure 5 is computed with the PWRC. It is distorted by artificial diffractions related to the discontinuous slope of the PWRC at the critical reflection angle (as in Figure 3). The vertical component computed with the ERC (Figure 6) is much smoother and does not contain artificial diffractions. The head waves are not clearly seen due to the limited length of the receiver array, which extends only up to the interference zone of the reflected and head waves. 3D modeling results with the ERC agree kinematically well the results obtained by finite-difference modeling and generalized ray tracing for the 2D model (Hanyga and Helle, 1995). Dynamically, the seismograms differ, in particular because of different geometrical spreading effects in 3D and 2D, as well as because of the influence of anisotropy.

Conclusions. We introduced effective reflection coefficients (ERC) for an interface between isotropic and TI media, and analyzed them for both plane and curved reflectors. In contrast to the conventional plane-wave reflection coefficients, the ERC depend on the frequency content of the seismic wavefield and the local reflector curvature. Our modeling results indicate that ERC may find applications in AVO studies of long-offset data and in Kirchhoff-type modeling.

Acknowledgements. M.A. is grateful to the Center for Wave Phenomena for support during her five-month visit to Colorado School of Mines. A.A. acknowledges the Russian Foundation for Basic Research (grant 07-05-00671). This work was partially funded by the Consortium Project on Seismic Inverse Methods for Complex Structures at the Center for Wave Phenomena.

References

Ayzenberg, M.A., Aizenberg, A.M., Helle, H.B., Klem-Musatov, K.D., Pajchel, J. and Ursin, B. [2007] Three-dimensional diffraction modeling of singly scattered acoustic wavefields based on the combination of surface integral propagators and transmission operators. *Geophysics*, **72**, SM19-SM34.

Hanyga, A. and Helle, H.B. [1995] Synthetic seismograms from generalized ray tracing. *Geophysical Prospecting*, **43**, 51-75.

Klem-Musatov, K.D., Aizenberg, A.M., Helle, H.B. and Pajchel, J. [2005] Reflection and transmission in multilayered media in terms of surface integrals. *Wave Motion*, **41**, 293-305.

Rüger, A. [2002] Reflection Coefficients and Azimuthal AVO Analysis in Anisotropic Media. *SEG*.

Tsvankin, I. [2005] Seismic Signatures and Analysis of Reflection Data in Anisotropic Media. *Elsevier*.

Van der Baan, M. and Smit, D. [2006] Amplitude analysis of isotropic P-wave reflections. *Geophysics*, **72**, C93-C103.

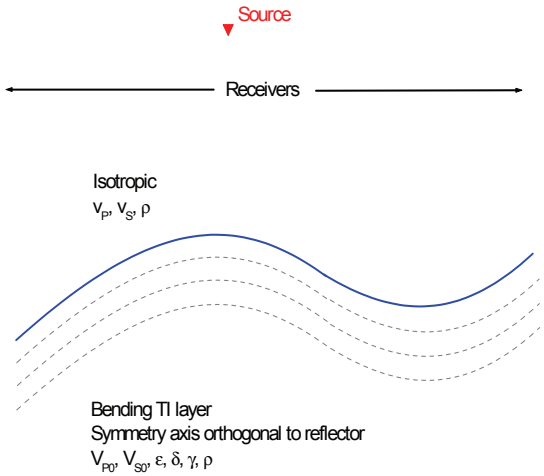

Figure 1: In-line section of the model.

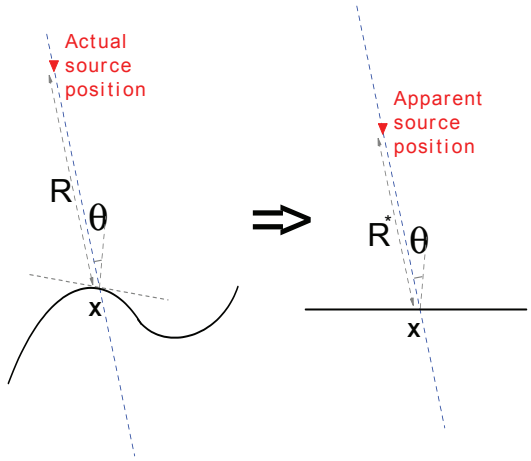

Figure 2: Actual and equivalent models.

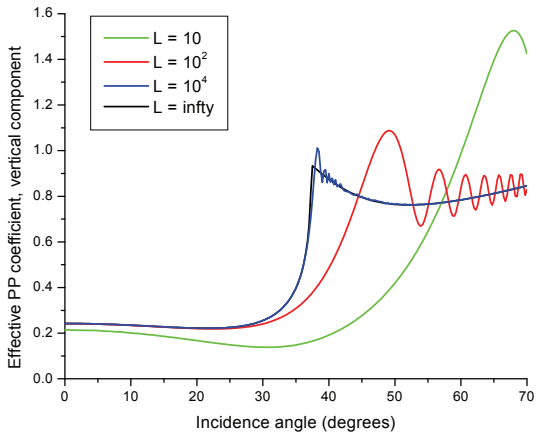

Figure 3: Absolute value of the PP ERC.

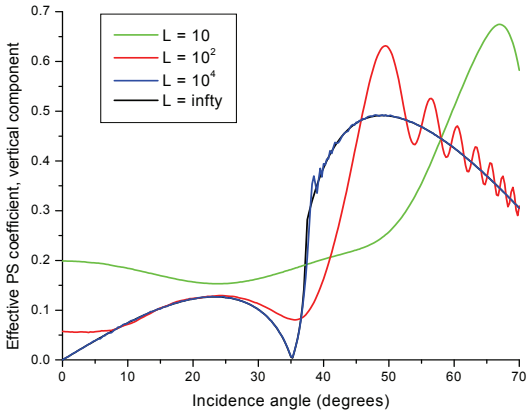

Figure 4: Absolute value of the PS ERC.

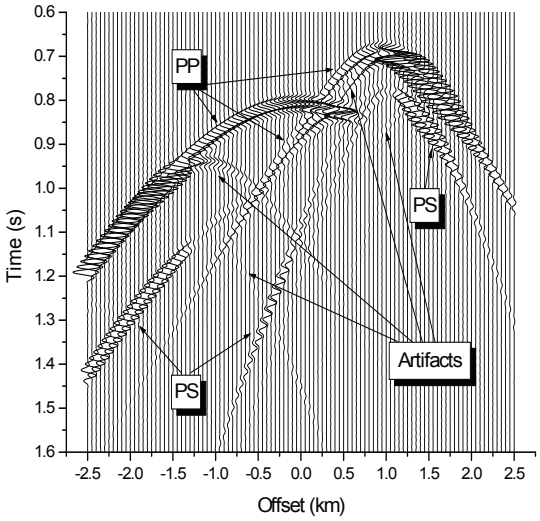

Figure 5: Seismogram computed with PWRC.

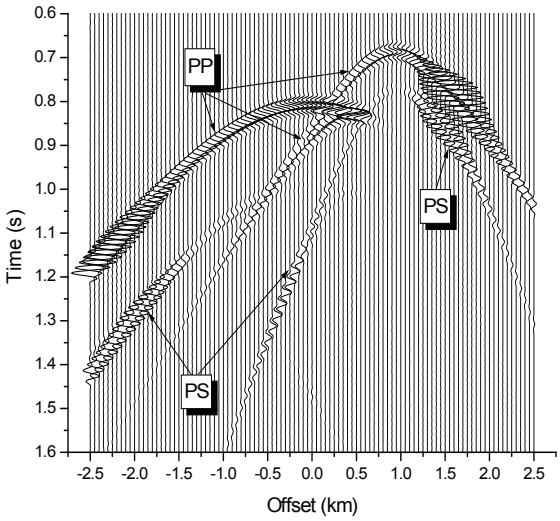

Figure 6: Seismogram computed with ERC.